REPORT DOCUMENTATION PAGE

Form Approved OMB NO. 0704-0188

1. REPORT DATE (DD-MM-YYYY)	2. REPORT TYPE	3. DATES COVERED (From - To)
18-01-2012	Final Report	15-Sep-2008 - 31-Mar-2011

4. TITLE AND SUBTITLE
Emission of Coherent Radiation from Ultra-High Mobility Carriers in Nano-structured Materials

5a. CONTRACT NUMBER

5b. GRANT NUMBER
W911NF-08-C-0126

5c. PROGRAM ELEMENT NUMBER
8G10AQ

6. AUTHORS
Andrew Iyengar, N. Convers Wyeth

5d. PROJECT NUMBER

5e. TASK NUMBER

5f. WORK UNIT NUMBER

7. PERFORMING ORGANIZATION NAMES AND ADDRESSES
Science Applications International Corporation-M
10260 Campus Point Drive
San Diego, CA 92121 -

8. PERFORMING ORGANIZATION REPORT NUMBER

9. SPONSORING/MONITORING AGENCY NAME(S) AND ADDRESS(ES)
U.S. Army Research Office
P.O. Box 12211
Research Triangle Park, NC 27709-2211

10. SPONSOR/MONITOR'S ACRONYM(S)
ARO

11. SPONSOR/MONITOR'S REPORT NUMBER(S)
55129-EL-DRP.1

12. DISTRIBUTION AVAILIBILITY STATEMENT
Approved for Public Release; Distribution Unlimited

13. SUPPLEMENTARY NOTES
The views, opinions and/or findings contained in this report are those of the author(s) and should not contrued as an official Department of the Army position, policy or decision, unless so designated by other documentation.

14. ABSTRACT
This report presents and analyzes a solid-state device concept for compact, dc-driven, room-temperature generation of coherent THz radiation. The advent of low-dimensional high-electron-mobility devices (HEMT) suggests that a micro-scale, solid-state analog of vacuum tube electron-beam microwave sources may be feasible.

15. SUBJECT TERMS
Terahertz radiation source, nanoscale, mode coupling

16. SECURITY CLASSIFICATION OF:			17. LIMITATION OF ABSTRACT	15. NUMBER OF PAGES	19a. NAME OF RESPONSIBLE PERSON
a. REPORT	b. ABSTRACT	c. THIS PAGE			N. Wyeth
UU	UU	UU	UU		19b. TELEPHONE NUMBER 000-000-0000

Report Title

Emission of Coherent Radiation from Ultra-High Mobility Carriers in Nano-structured Materials

ABSTRACT

This report presents and analyzes a solid-state device concept for compact, dc-driven, room-temperature generation of coherent THz radiation. The advent of low-dimensional high-electron-mobility devices (HEMT) suggests that a micro-scale, solid-state analog of vacuum tube electron-beam microwave sources may be feasible.

Enter List of papers submitted or published that acknowledge ARO support from the start of the project to the date of this printing. List the papers, including journal references, in the following categories:

(a) Papers published in peer-reviewed journals (N/A for none)

Received Paper

TOTAL:

Number of Papers published in peer-reviewed journals:

(b) Papers published in non-peer-reviewed journals (N/A for none)

Received Paper

TOTAL:

Number of Papers published in non peer-reviewed journals:

(c) Presentations

Number of Presentations: 0.00

Non Peer-Reviewed Conference Proceeding publications (other than abstracts):

Received Paper

TOTAL:

Number of Non Peer-Reviewed Conference Proceeding publications (other than abstracts):

Peer-Reviewed Conference Proceeding publications (other than abstracts):

Received Paper

TOTAL:

Number of Peer-Reviewed Conference Proceeding publications (other than abstracts):

(d) Manuscripts

Received Paper

TOTAL:

Number of Manuscripts:

Books

Received Paper

TOTAL:

Patents Submitted

Patents Awarded

Awards

Graduate Students

NAME	PERCENT_SUPPORTED

FTE Equivalent:
Total Number:

Names of Post Doctorates

NAME	PERCENT_SUPPORTED

FTE Equivalent:
Total Number:

Names of Faculty Supported

NAME	PERCENT_SUPPORTED

FTE Equivalent:
Total Number:

Names of Under Graduate students supported

NAME	PERCENT_SUPPORTED

FTE Equivalent:
Total Number:

Student Metrics

This section only applies to graduating undergraduates supported by this agreement in this reporting period

The number of undergraduates funded by this agreement who graduated during this period:	0.00
The number of undergraduates funded by this agreement who graduated during this period with a degree in science, mathematics, engineering, or technology fields:.....	0.00
The number of undergraduates funded by your agreement who graduated during this period and will continue to pursue a graduate or Ph.D. degree in science, mathematics, engineering, or technology fields:.....	0.00
Number of graduating undergraduates who achieved a 3.5 GPA to 4.0 (4.0 max scale):	0.00
Number of graduating undergraduates funded by a DoD funded Center of Excellence grant for Education, Research and Engineering:	0.00
The number of undergraduates funded by your agreement who graduated during this period and intend to work for the Department of Defense	0.00
The number of undergraduates funded by your agreement who graduated during this period and will receive scholarships or fellowships for further studies in science, mathematics, engineering or technology fields:	0.00

Names of Personnel receiving masters degrees

NAME

Total Number:

Names of personnel receiving PHDs

NAME

Total Number:

Names of other research staff

NAME PERCENT_SUPPORTED

FTE Equivalent:

Total Number:

Sub Contractors (DD882)

Inventions (DD882)

Scientific Progress

Table of Contents

Technology Transfer

REPORT DOCUMENTATION PAGE
Form Approved
OMB No. 0704-0188

1. REPORT DATE ***(DD-MM-YYYY)***
31-03-2011
2. REPORT TYPE
Final Progress Report
3. DATES COVERED ***(From - To)***
8/28/2008 – 3/31/2011
4. TITLE AND SUBTITLE
Emission of Coherent Radiation from Ultra-High Mobility

5a. CONTRACT NUMBER
W911NF-08-C-0126
Carriers in Nano-structured Materials

5b. GRANT NUMBER

5c. PROGRAM ELEMENT NUMBER

6. AUTHOR(S)

5d. PROJECT NUMBER

Iyengar, Andrew
Wyeth, N. Convers

5e. TASK NUMBER

5f. WORK UNIT NUMBER

7. PERFORMING ORGANIZATION NAME(S) AND ADDRESS(ES)

AND ADDRESS(ES)
8. PERFORMING ORGANIZATION REPORT
NUMBER
Science Applications International Corp.

1710 SAIC Drive
McLean, VA 22012

9. SPONSORING / MONITORING AGENCY NAME(S) AND ADDRESS(ES)
10. SPONSOR/MONITOR'S ACRONYM(S)

DSO/DARPA
Defense Sciences Office

DARPA

11. SPONSOR/MONITOR'S REPORT
3701 N. Fairfax Drive

NUMBER(S)
Arlington, VA 22203

12. DISTRIBUTION / AVAILABILITY STATEMENT

13. SUPPLEMENTARY NOTES

14. ABSTRACT
This report presents and analyzes a solid-state device concept for compact, dc-driven, room-temperature generation of coherent THz radiation. The advent of low-dimensional high-electron-mobility devices (HEMT) suggests that a micro-scale, solid-state analog of vacuum tube electron-beam microwave sources may be feasible.
15. SUBJECT TERMS
Terahertz radiation source, nanoscale, mode coupling
16. SECURITY CLASSIFICATION OF:

17. LIMITATION
OF ABSTRACT
18. NUMBER OF PAGES
19a. NAME OF RESPONSIBLE PERSON

a. REPORT
U
b. ABSTRACT
U
c. THIS PAGE

U
UU
33

19b. TELEPHONE NUMBER *(include area code)*

Standard Form 298 (Rev. 8-98)
Prescribed by ANSI Std. Z39.18

(1) No submissions or publications under ARO sponsorship during this reporting period.

(2) No Student/Supported Personnel Metrics

(3) No Technology transfer activities to date

(4) No other technical reports due to ARO.

Emission of Coherent Radiation from Ultra-High Mobility Carriers in Nano-structured Materials

Final Report
DARPA Contract No. W911NF-08-C-0126

Dr. Andrew Iyengar and Dr. N. Convers Wyeth

31 March 2011

Table of Contents

Foreword

This project was initiated by SAIC scientist Dr. Spilios Riyopoulos, who recognized that bringing together long-established concepts from plasma physics with cutting-edge nanostructured materials could lead to a new compact, DC-powered source of coherent THz radiation. Due to his untimely passing, he had the opportunity neither to complete the contract nor see his ideas realized in a working device. Section 1 is based primarily on his published and unpublished manuscripts as well as other available documentation of his work on the project. The authors resumed work on the contract in the summer of 2010, and our contribution is covered in the remaining sections of the report. Our approach has deviated in many ways from Riyopoulos' initial formulation. Nonetheless, we continue to rely on his original insights and are glad to have brought his ideas closer to fruition.

1 THz lasing from hybrid modes

1.1 Introduction

The terahertz (THz) part of the electromagnetic spectrum, with frequencies spanning 0.1-1.0 THz, stands out as being relatively technologically underdeveloped despite wide-ranging and important potential applications. These include high-resolution stand-off detection for security and medical imaging of soft tissues. Certain excitations of complex molecules fall into the THz regime, leading to spectroscopy applications in molecular biology, chemistry, and pharmaceuticals. THz radiation suffers little attenuation in the atmosphere due to fog, rain, or suspended particulates as opposed to optical and infrared radiation, suggesting potential applications in radar, long-range imaging, and short-range telecommunications.

Table 1.1. Comparison of Available THz Sources.

THz Source		Coherent	CW	Tunable	Power	Efficiency	Room T	Cost	Size
Electronic Upconversion	Gunn diode cascades	No	Yes	Yes	mW	< 1 %	Yes*	$$$	Small
	Tunnel diode cascades	No	Yes	Yes	mW	< 1 %	Yes*	$$$	Small
Optical Downconversion	Two wave beating	Yes	Yes	No	μW	< 0.1 %	Yes	$$$	Med-Large
	Pulsed Ti:Sh	No	No	No	μW	< 0.1 %	Yes	$$$	Med-Large
Quantum Cascade Lasers		Yes	Yes	No	mW	few %	No	$$	Small
Backward Oscillators		Yes	Yes	Yes	mW	< 1 %	Yes	$$	Large
Free Electron Lasers		Yes	Yes	Yes	kW	few %	Yes	$$$$$	HUGE

The lack of compact, room-temperature, low-cost sources of coherent THz radiation has hindered the development of THz technology. Table 1.1 compares some available technologies for generating THz radiation. One approach is indirect: up- or down- conversion of radiation from the neighboring microwave and optical frequency ranges. On the microwave side, such sources suffer from poor efficiency and a lack of phase coherence. On the optical side, devices are large, and efficiency and total output power drop considerably. Direct generation at THz frequency is possible in solid-state quantum cascade lasers (QCLs) which, however, are not frequency-tunable and operate only at cryogenic temperatures. There are also gas lasers based on methanol line emission (2.5 GHz) which require pumping by an external laser. Direct THz generation can also be obtained from a free electron beam interacting with a slow-

wave structure. These devices include klystrons, traveling wave tubes (TWTs), backward wave oscillators (BWOs), and free electron lasers (FELs). They offer frequency tunability and better control, efficiency, and output characteristics, but are prohibitively large and/or expensive for many applications.

This study aims to combine the coherent, tunable, CW, high-power characteristics of backward oscillators and free electron lasers with the compactness, portability, low cost, and high power density of a solid state device. This report presents and analyzes concepts for generating of coherent THz generation from streaming charge carriers in a solid-state device. Electrons in the solid state offer several advantages over the free electron beams utilized in BWOs, TWTs, and FELs. The ions of the solid provide a neutralizing charge background, allowing for strong confinement of the charges and high current densities. On the other hand, the phase coherence of electrons in bulk semiconductors is destroyed by collisions with impurities, other electrons, and lattice vibrations. This collision time is typically much shorter than the radiation time, placing practical device efficiencies out of reach.

A new class of materials, combining ultra-high carrier mobility with low carrier dimensionality, offers radiation times comparable to or longer than the collision time. This suggests the possibility of efficient conversion of streaming carrier energy into coherent radiation, leading to a nanoscale analog of beam-powered coherent microwave sources. This report analyzes the possibility of basing such devices on the two-stream instability, a well-known idea from plasma physics. This instability converts the kinetic energy of two charge systems drifting relative to one another into an oscillation of charges and electromagnetic fields, which in turn can emit coherent radiation into free space.

We contemplate using ultra-high mobility (UHM) materials are based on either doped polar semiconductors or carbon. While two-dimensional confinement of an electron gas has long been possible in polar semiconductor heterostructures, one-dimensional analogs are now available in arrays, illustrated in Figure 1-1. These core-shell structures trap a UHM cylindrical electron gas at the interface between p-type core and n-type coating. Nanometer-scale confinement is possible in metallic carbon nanotubes and graphene, which offer, respectively, one- and two-dimensional confinement of UHM carriers at room temperature. These materials also have a unique band structure that endows electrons with a linear dispersion relation as well as a chiral property that suppresses backscattering.

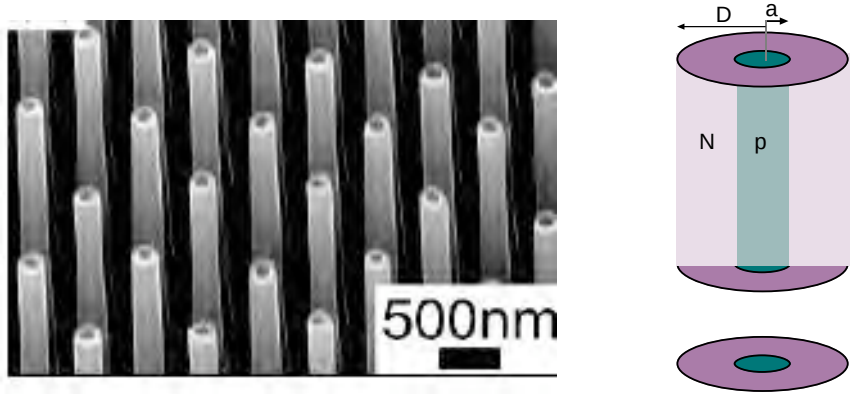

Figure 1-1. Image and schematic view of one-dimensional core-shell semiconductor nanorods.

Our concept differs from other solid state approaches. In quantum cascade lasers, carriers emit radiation when moving across band energy steps in real space. The spacing of these steps is built into the device and determines the radiation wavelength, meaning that the wavelength is not tunable. In our approach, carriers radiate continuously at a frequency determined by their velocity, allowing the frequency to be tuned via the drift current. Another approach is voltage-tunable and based on the

Dyakonov-Shur instability[1], in which gain is substantially lower and occurs only upon reflection from drain boundaries of the device. In our approach, the oscillation mode is amplified in transit as it propagates parallel to the drift current. This makes our device concept a true analog to microwave electron beam devices. There has been recent progress in generating THz radiation from miniaturized traveling wave tubes, but the solid state nanostructures contemplated herein promise much smaller sizes and higher current densities.

It is well known from plasma physics[2] that charged "fluids" in relative motion are unstable to the growth of oscillations. Consider one uniform charged fluid initially at rest and another uniformly charged fluid moving with velocity u. Both fluids individually support plasma oscillations due to their interaction with the electromagnetic field. These oscillations require energy of at least ω_p, the plasma frequency, and thus do not occur spontaneously. On the other hand, together the two fluids exchange energy, converting the energy of relative motion into a collective plasma oscillation that grows exponentially. The situation is illustrated in Figure 1-2. We refer to this collective oscillation as a "hybrid mode", as it involves the oscillating motion of both charge fluids along with oscillating electromagnetic fields. In a longitudinal hybrid mode (as shown in the figure), both the direction of both mode propagation and charge oscillation is parallel to the drift direction. In a transverse mode the oscillation is transverse to u.

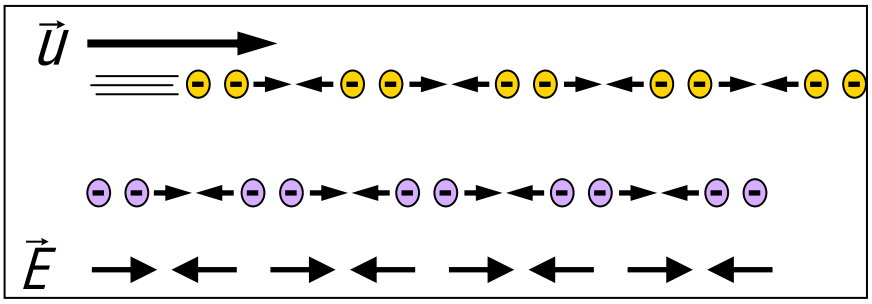

Figure 1-2. Two charged fluids, one stationary (violet) and one moving (yellow) interact to produce a (longitudinal, in this example) oscillation of charge densities and fields. These "hybrid" mode oscillations occur regardless of the sign of the charge in either fluid.

Our proposal is based on this two-stream instability*. The role of the moving charged fluid is provided by electron/hole carriers in a solid state nanostructure. In real materials, carriers are accelerated by an external electric field until they lose energy, either by radiation or by colliding with impurities, other electrons, or ion lattice vibrations (phonons). Although high current densities are possible in the solid state, these collisions are ordinarily incoherent and compete with radiation processes, damping the oscillation. The challenge, then, is to reduce this collision rate so that it is less than or comparable to the radiation rate.

* In contrast, the Dyakonov-Shur mechanism is a "one-stream" instability.

In semiconductor devices, phonons typically dominate other scattering mechanisms. One way to deal with phonon collisions is to limit the scattering phase space by confining carriers to low dimensions. Another approach is to stimulate the emission of coherent phonons. Effectively, the lattice ions themselves constitute the second charged "fluid" in the two-stream instability. Electron-phonon collision

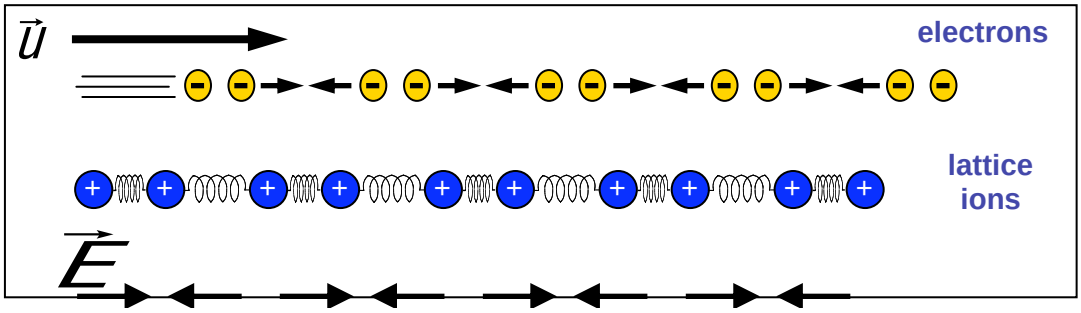

Figure 1-3. Components of the 3P hybrid mode.

processes, ordinarily incoherent, are dominated by coherent collisions occurring in phase with the electron plasma oscillation. Electron-phonon collisions become part of the radiating mode, rather than competing with it. The situation is illustrated in Figure 1-3. We refer to this particular hybrid mode as a plasmon-phonon-polariton (3P) mode, which name refers to the oscillation of electron charge density, ion charge density, and electromagnetic field.

This report is organized as follows: the remainder of Section 1 gives an overview of the work of S. Riyopoulos analyzing the 3P mode using the methods of plasma physics. In Section 2, we identify methods from condensed matter physics that address some of the shortcomings of the plasma physics approach in relation to realistic solid state materials. We also introduce a framework for understanding the conditions for mode amplification independent of whether or not phonons play the role of the second charged fluid in the instability. Section 3 identifies metallic carbon nanotubes (mCNTs) as a testing ground for the practicability of the 3P mode idea. From the experimental and theoretical literature on mCNTs at high bias, we conclude that efficient amplification of a coherent 3P mode is unlikely to be realized in mCNT devices. In Section 4, we propose periodic metal films (PMFs) and the associated surface plasmons as a practical alternative to phonons. We argue that combining existing PMF technologies with high-electron-mobility transistors (HEMTs) can provide a high-Q cavity with round-trip amplification of THz radiation at room temperature. We identify realizable device parameters and discuss the anticipated performance characteristics. Section 5 summarizes our findings.

1.2 Classical analysis of the 3P mode

A classical analysis of the 3P mode was undertaken by S. Riyopoulos both prior to[3] and under[4,5] the present contract. At the simplest level, the electrons can be regarded as a charged fluid, which description is valid when the drift velocity is much larger than the thermal velocity spread $\sqrt{k_B T_e / m_e *}$, where T_e and m_e are the electron effective temperature and band mass, respectively. In high-electron-mobility semiconductors, the two-fluid instability can, in principle, be realized between conduction electrons and valence holes. Most of the drift current under bias is sustained by the electrons, as they have much higher mobility, and the holes are effectively stationary. In practice, a strongly P- or N-doped semiconductor has a prohibitively small density of one type of carrier, whereas electrons and holes in a P-N junction will likely be lost to various recombination processes.

1.2.1 Cold fluid dispersion

If there are two separate charged species, specifically electrons and lattice ions, charges are not lost to recombination. Ions can be modeled as harmonic oscillators about fixed positions driven by the electric field. For a three-dimensional "cold" fluid of classical electrons, in which thermal deviations from the average velocity *u* are negligible, the equation for sinusoidal oscillations (with complex longitudinal fields varying as $e^{i(kz-\omega t)}$) is

$$1-\frac{\omega_e^2}{(\omega-ku)^2}-\frac{\omega_A^2}{\omega^2-\Omega_A^2}=0\,.$$

where ω_e is the electron plasma frequency, ω_A is the ion plasma frequency, and Ω_A is the resonant frequency of the ion oscillators. The solution is a dispersion relation $\omega(k)$ with four branches, two of which are real-valued. The other two branches are either both real- or both complex-valued. The latter case implies the presence of one damped (Im ω < 0) and one unstable (Im ω > 0) mode. The unstable mode continuously converts drift energy into an oscillation with exponential growth in time. An unstable mode exists whenever

$$ku>\Omega_A$$

and either

$$ku\le\omega_e\Omega_A/\omega_A \quad \textbf{or} \quad ku>\left|\omega_e-ku\right|>\sqrt{\omega_A^2+\Omega_A^2}\,,$$

and exponential growth occurs for wavevectors *k* such that

$$ku\ge\omega\,.$$

Further analysis shows that growth rates comparable to the frequency can be obtained for frequencies in the range 0.1-1.0 THz with optical phonons and high electron densities (i.e. the electron plasma frequency also lies in the 0.1-1.0 THz range.) The parameter Ω_A can be identified as the transverse optical phonon frequency ω_{TO}, and the longitudinal optical phonon frequency is given by

$$\omega_{LO}=\sqrt{\omega_{TO}^2+\omega_A^2}\,.$$

There is also a transverse plasma oscillation mode, for which the instability cannot be realized in a device because the drift velocity must exceed the material speed of light.

1.2.2 Thermal effects

The effect of thermal velocity spreads can be calculated using the Maxwell-Boltzmann kinetic equation. These spreads reduce, but do not eliminate, the growth rate, which is present whenever

$$\omega_{TO}<ku<\omega_{LO}.$$

Given a narrow carrier velocity distribution $f(u)$, the growth rate for a mode with phase velocity *v* varies approximately as $df/du|_{u=v}$. This is because strong emission occurs for carriers moving slightly faster than *v*, while strong absorption occurs for carriers moving slightly slower than *v.* Riyopoulos gives a detailed analysis of these thermal as well as oblique and transverse-polarization modes. Large growth rates require that a substantial fraction of carriers resonate with the lasing mode. Wideband semiconductor materials are identified as having promising properties (effective mass, carrier density, and optical phonon frequency) appropriate for dc to terahertz generation.

2 Solid State Analysis

The previous section analyzes the amplification of a hybrid mode from the perspective of plasma physics. Electrons are assumed to behave classically and as free particles moving in three dimensions. Similarly, lattice ions are viewed as masses oscillating about a fixed position with a linear restoring force. In this section, we discuss how to generalize the analysis to account for important features in solid state nanostructures. The crystalline lattice imposes bandstructure on both electrons and phonons, important for understanding the strength of the electron-phonon interaction. High carrier densities and low temperatures require the use of quantum statistics for electrons. We are also interested in reduced dimensionality. Finally, quantum mechanical fluctuations can dramatically change the behavior of electrons and phonons in real materials. In the following, we show how to formally account for these features in the hybrid mode analysis.

We should first point out that we do not attempt a fully quantum mechanical treatment of the problem. We take the approach that the electromagnetic field behaves classically, computing the *linear* response of the solid state system to classical electromagnetic fields using the methods of quantum statistical mechanics. In effect, we are accounting for stimulated emission and absorption and neglecting spontaneous radiation processes. We will eventually make approximations that also discard incoherent electron-phonon processes. Coherent and incoherent phonon amplitudes in semiconductors have been analyzed in connection with the excitation of coherent phonons by optical pulses[6].

Although rigorous methods exist for quantum statistical mechanics in the non-equilibrium context[7], we take the very simple approach of using equilibrium methods with presumed non-equilibrium carrier distributions. Non-equilibrium methods are needed to predict carrier momentum distributions and spatial inhomogeneities in the steady state and to understand gain saturation. We defer such analysis to future work and parameterize the (unknown) carrier distribution in our calculations in terms of an effective drift velocity and carrier temperature.

2.1 Linear response in equilibrium

We consider a spatially uniform solid state system with dimensionality *d* which is perturbed by a small electrostatic potential $\Delta\varphi$ which may vary in time and space. The perturbation produces space- and time-dependent changes in the charge density $\Delta\rho$. We define the linear response kernel *K* in Fourier space by

$$\Delta\rho(q,\omega) = \Delta\phi(q,\omega)\ K(q,\omega)$$

On the other hand, Poisson's equation reads

$$\Delta\rho(q,\omega)/\varepsilon_1 = \Delta\phi(q,\omega)/V_C(q)$$

where $V_C(q)$ is the Coulomb potential in the Fourier domain, ε_1 is a background dielectric constant. Although the Coulomb potential in *real* space always varies as $1/r$, the Fourier transform is computed using the dimensionality *d* of the charge system. The Coulomb potential in various dimensions is

$$\tilde{V}_C(r) = \frac{1}{4\pi\varepsilon_1 |r|} \rightarrow V_C(q) = \begin{cases} \dfrac{1}{\varepsilon_1 |q|^2} & \text{for } d = 3 \\ \dfrac{1}{2\varepsilon_1 |q|} & \text{for } d = 2 \\ \dfrac{K_0(qa)}{2\pi\varepsilon_1} & \text{for } d = 1 \end{cases}$$

where K_0 is a modified Bessel function. For the Fourier transform to converge in one dimension, we must introduce an effective system width a. Dimensionality changes the small-q (i.e. long-range) behavior of the Coulomb interaction and plays an important role in the long-wavelength behavior of plasma oscillations. The dispersion relation $\omega(q)$ for these plasma oscillations is given by the above equations for $\Delta\varphi$ and $\Delta\rho$, which also gives us the expression for the dielectric function:

$$\varepsilon(q,\omega)/\varepsilon_0 = 1 - V_C(q)\,K(q,\omega) = 0\,.$$

The linear response K is given in real space by the Kubo formula in terms of the quantum-statistical correlation function

$$K(q,\omega) \leftarrow \tilde{K}(x - x', t - t') = \left\langle \hat{\rho}(x,t)\hat{\rho}(x',t') \right\rangle,$$

where ρ is the quantum mechanical operator for total charge density. The total charge includes contributions from both electrons and ions. This correlation function can be computed, including temperature effects, by diagrammatic techniques of quantum statistical mechanics[8]. The inclusion of various kinds of diagrams can account for electron-electron, electron-phonon, and phonon-phonon interactions at varying levels of approximation.

Calculating the effects of electron-phonon interaction is a difficult undertaking, and there is a considerable literature on the subject. The effective interaction differs from the classical analysis of Section 1 in several important ways. The single-particle states of electrons and phonons are described by Bloch wavefunctions and normal modes of oscillation, respectively. The effective strength of electrostatic interaction between particular electron and phonon states and be substantially reduced (and for highly symmetric crystals, even be made to vanish) by the details of their spatial eigenfunctions. Screening of the Coulomb force by charge flows is strongly affected by virtual processes, which are fundamentally quantum mechanical. Predictions of electron-phonon coupling are thus highly material-dependent and require considerable theoretical and computational effort.

A typical approach is to separate all contributions to the dielectric function involving phonons into a separate term, which is then given a phenomenological approximation. An optical phonon branch can be regarded, in the simplest approximation, as non-dispersing, and a typical parameterization for the dielectric response is

$$\varepsilon(q,\omega)_{\text{phonon}} = \varepsilon_\infty \frac{\omega^2 - \omega_{\text{LO}}^2 + i\Gamma}{\omega^2 - \omega_{\text{TO}}^2 + i\Gamma},$$

where ω_{LO} and ω_{TO} are the longitudinal and transverse optical phonon frequencies, respectively. The approach of Section 1 described the phonons in the same way, albeit with $\Gamma = 0$. The decay rate Γ reflects the fact that phonons in real materials have a finite lifetime. The effective potential for ions oscillating in the lattice is not exactly harmonic, and the anharmonicity gives rise to a decay rate Γ for optical phonons to decay into two or more acoustic phonons. A non-equilibrium optical phonon population therefore tends to thermalize into a "heat bath" of acoustic phonons.

The remaining contributions to the dielectric function come from electrons alone, and are given by

$$\left\langle \hat{\rho}_{\mathrm{el}}(x,t)\hat{\rho}_{\mathrm{el}}(x',t')\right\rangle \rightarrow K_{\mathrm{el}}(q,\omega) = -\frac{e^2}{\hbar}\Pi(q,\omega)$$

where ρ_{el} is the electron charge density operator, e is the electron charge, and Π is the electron polarizability. At this point the random phase approximation (RPA) is commonly used, replacing Π by its non-interacting value Π_0. For a single carrier band, it is given by

$$\Pi_0(q,\omega) = 2\int \frac{d^d k}{(2\pi)^d}\frac{f(E_k) - f(E_{k+q})}{E_k - E_{k+q} - \omega}$$

where f is the Fermi-Dirac distribution for temperature T and chemical potential μ, and E_k is the dispersion relation for the band*. The case of a quadratically dispersing band, the analysis of $\Pi_{0\ has}$ been carried out in various temperature limits in the literature. At zero temperature and d = 3, the result gives rise to the Lindhard dielectric function. In the classical limit, one recovers the results of the classical Boltzmann approach used in plasma physics. The polarization for multiband systems can be derived from the above definition of K_{el} and includes contributions from interband transitions.

2.2 Analysis of the dielectric function

Before looking at the effects of drifting carriers, we first consider how to analyze the dielectric function to obtain useful information about amplification of the hybrid mode. In the approach of Section 1, the growth rate of plasma oscillations was determined by finding the complex zeros of the full dielectric function, including electron and phonon contributions. In this section, we aim for a more flexible approach that allows us to determine whether gain is possible from drifting carriers without specifying the properties of the second system (phonons).

Rather than finding the exact growth or decay rates of oscillations, we aim to identify q-ω regions of resonant energy exchange with electromagnetic fields. Such resonance occurs for real q and ω when

$$\mathrm{Re}\,\varepsilon(q,\omega) = 0\,,$$

where ε contains the dielectric response of electrons and phonons. We consider the real-valued dispersion relation $\omega(q)$ from this equation, rather than the complex-valued one given by the complex zeros of ε. The rate of energy transfer to the fields is related to the imaginary part. When the gain or loss rate is small relative to the frequency, the growth rate G of electromagnetic field energy is given by[9]

$$G(q,\omega) = -2\frac{\omega\,\mathrm{Im}\,\varepsilon(q,\omega)}{\dfrac{d}{d\omega}\mathrm{Re}[\omega\,\varepsilon(q,\omega)]}\,.$$

Along the resonance curve $\omega(q)$, we have

$$G(q,\omega) = -2\frac{\mathrm{Im}\,\varepsilon(q,\omega)}{\dfrac{d}{d\omega}\mathrm{Re}[\,\varepsilon(q,\omega)]}\,.$$

* Graphene and carbon nanotubes have an additional chirality factor in the integrand, c.f. S. Das Sarma and E. H. Hwang, *Phys. Rev. Lett.* **102**, 206412 (2009)

Positive contributions to the imaginary part of the dielectric function arise from processes which damp propagating electromagnetic fields. Similarly, negative contributions reflect gain. Analyzing the electronic contribution to Im ε will give us insight into the gain space for drifting carriers. Even if we neglect damping by the phonons, we cannot evaluate G without them, since the ion dielectric response in part determines the resonance dispersion relation and Re ε. On the other hand, we can evaluate the oscillator strength for electrons alone, given by

$$F(q,\omega) = \omega \,\mathrm{Im}\, \varepsilon_{\mathrm{el}}(q,\omega)/\varepsilon_0 \,,$$

which allows us to identify the important regions of the gain space. Besides the connection to the growth rate, F has, in equilibrium, the important property

$$\frac{2}{\pi}\int_0^\infty F(q=0,\omega)\; d\omega = \frac{ne^2}{m^*} \quad ,$$

a result known as the oscillator strength sum rule. This powerful result holds independent of temperature and any interaction effects.

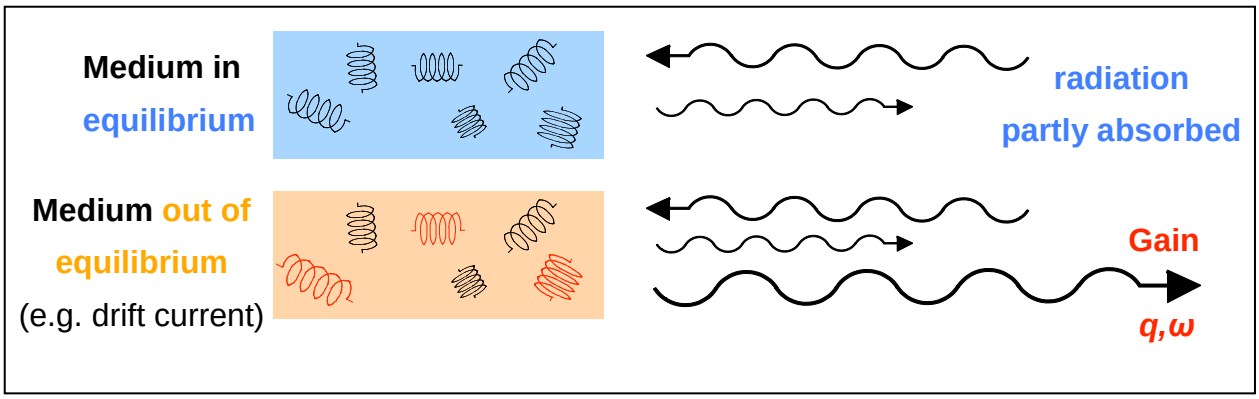

Figure 2-1. A medium in equilibrium absorbs energy from the electromagnetic field. Out of equilibrium, the medium can transfer energy to the field in particular regions of q-ω space, where F is negative.

One way to understand the oscillator strength concept is illustrated in Figure 2-1. The charge response of the system can be visualized as a collection of damped harmonic oscillators, one for each value of q, each of which is driven periodically by the electromagnetic field. The sign of F tells us whether energy is transferred to the oscillator from the field or vice versa when driven at frequency ω. In equilibrium, F is always positive, and all oscillators absorb energy from the field. Out of equilibrium, however, *some* oscillators transfer energy *to* the field, resulting in amplification of the electromagnetic wave. An analysis of F in the non-equilibrium system will show the direction and magnitude of energy transfer as a function of q and ω. This provides a "gain map", allowing the design of a hybrid mode that maximizes gain.

2.3 Drifting carriers

To handle carrier drift, we modify the expression for Π_0 by altering the momentum distribution of carriers, contained in the Fermi-Dirac functions f. For a single band with quadratic dispersion and mass m^*, we simulate a carrier drift velocity u by making the substitution

$$f(E_k) \rightarrow f(E_{k-m^*u}) \,,$$

and similarly for $f(E_{k+q})$. Generally, the chemical potential must change with u to keep the carrier density fixed. In the non-equilibrium setting, T should be regarded as an *effective* carrier temperature that characterizes the steady-state distribution of occupied electronic states.

2.3.1 Zero-temperature electron gas

Oscillator strength $F(k,\omega)$ for a drifting electron gas at zero temperature is shown in Figure 2-2, for k parallel to the drift velocity. This limit best shows the role of Fermi statistics. Frequency and temperature are scaled by the Fermi wavevector k_F and Fermi energy E_F, respectively, and the drift velocity is $u = v_F/2$. The dashed line shows the slope associated with the drift velocity, and the green line shows the resonance curve Re $\varepsilon = 0$.

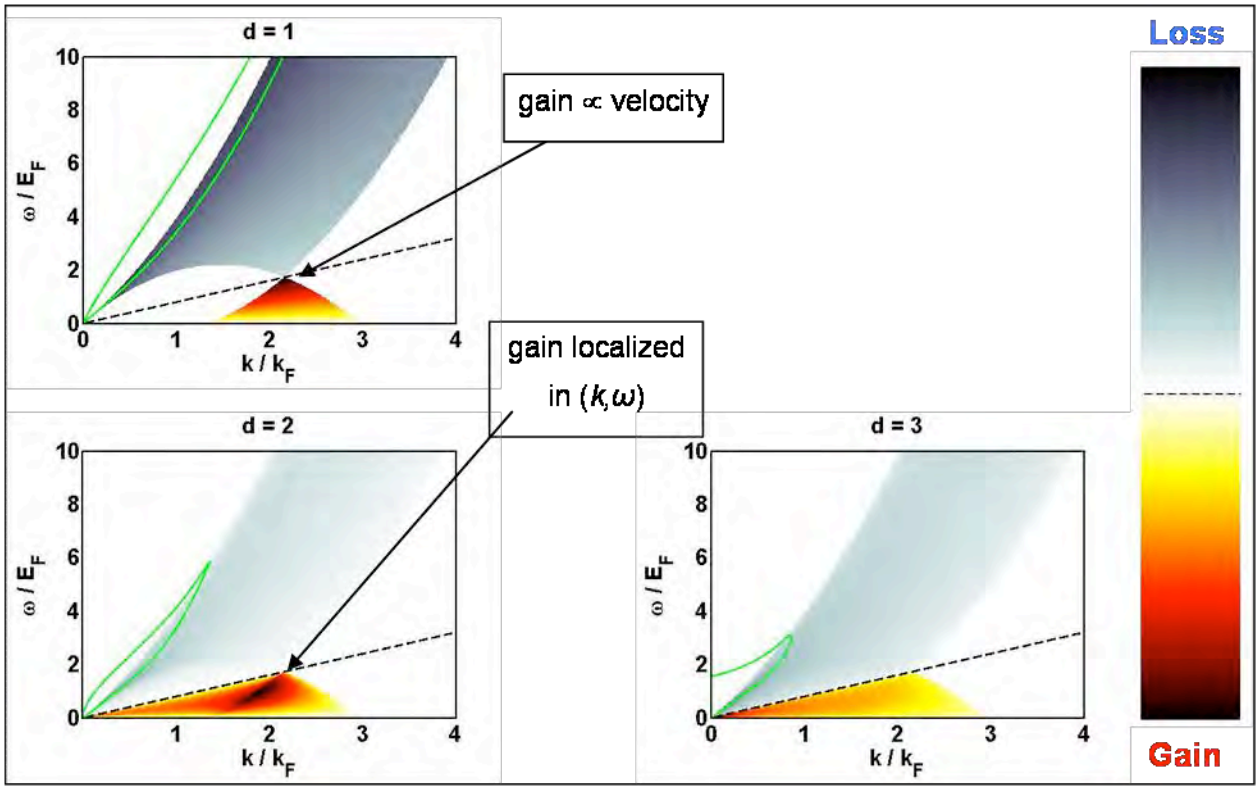

Figure 2-2. Oscillator strength F(k,ω) at zero temperature for a free electron gas. Drift velocity (black, dashed), is v_F / 2. The dispersion curve for plasma oscillations is shown in green.

The most important consequence of Fermi statistics is presence of large regions of zero oscillator strength (white), where the Pauli exclusion principle prevents electrons (to leading order) from absorbing or emitting radiation. In one dimension, there is a forbidden zone (white, below the particle-hole continuum) not found in higher dimensions due the extreme kinematic restrictions on electron scattering. Absorption is diminished in this region for $d = 2$ and to a lesser extent for $d = 3$. As expected, gain only occurs when the phase velocity is lower than the drift velocity. However, the distribution of the gain region depends on dimension. For $d = 1$, gain depends only on the phase velocity, whereas it is localized in k and ω for $d = 2$. In three dimensions, the gain is diffusely distributed. We conclude that at low temperatures (more precisely, for a degenerate electron gas), low dimensionality concentrates the gain region in k-ω space, which may help to optimize gain and bandwidth in a practical device.

The plasma wave dispersion is shown in green, and we recover the well-known results that plasma oscillations are gapped for d = 3 and have a maximum frequency for d = 2, 3. Note that one dispersion branch lies in a forbidden region and another in a loss region. The former is a stable propagating mode, whereas the latter quickly decays as it transfers energy to electron-hole excitations. Note that the resonance curve does not intersect the gain region. We find this to be true regardless of the size of the drift velocity. This highlights the fact that the role of the second charged system is to provide a branch of the plasma wave dispersion which intersects the gain region, providing the desire amplified mode.

We may, in fact, design the second charge system (i.e. choose phonon parameters) that place this intersection in the region of maximum gain. This is illustrated in Figure 2-3 for d=1, where we include a phenomenological phonon term in the dielectric function (*without* anharmonic phonon decay). The localization of the gain region implies that an amplified mode occurs suddenly only above a critical drift velocity $u > u_C \approx \omega_{LO}/(2k_F)$.

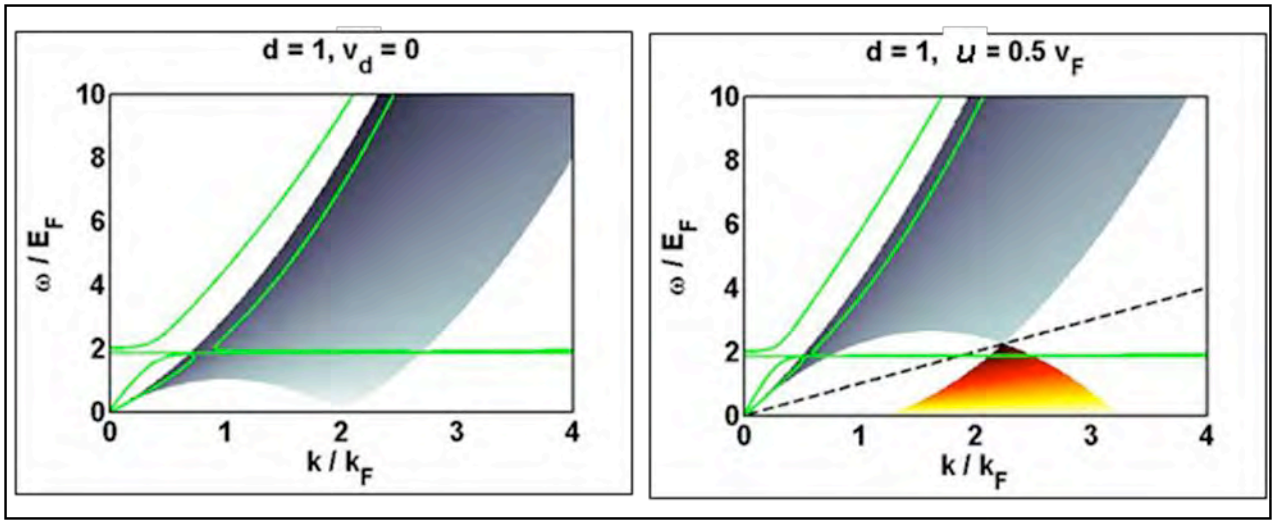

Figure 2-3. Oscillator strength and dispersion curves (green) for u = 0(left), u=v_F/2 (right) for a d=1 electron gas coupled to an optical phonon. An amplified mode appears for $u > u_C \approx \omega_{LO}/(2k_F)$.

2.3.2 Classical electron gas

In the classical limit, the Fermi-Dirac distribution can be replaced by a Boltzmann distribution:

$$f(E) \to e^{-[E-\mu]/k_BT}.,$$

The result for Π_0, expressed in terms of the d-dimensional carrier density n, is *independent* of dimension and given by the so-called "plasma-dispersion" function. Classically, the components of momentum orthogonal to the drift current, both of the carriers and of the radiation field, are irrelevant. The oscillator strength, though, also depends on $V_C(q)$, which does depend on dimension.

We focus our attention on d = 2, which is needed for our device proposal in Section 4. Again we assume q parallel to the drift velocity. It is convenient to express F using the phase velocity $v = \omega/q$, the drift velocity u, the "thermal" velocity $v_T = (2\,k_BT/m^*)^{1/2}$, and the scaled frequency $w = \hbar\omega/k_BT$.

$$F(q,\omega) = -\frac{\sqrt{\pi}e^2}{\varepsilon_0\hbar}\frac{n}{\varepsilon_r}\frac{v^2}{\omega v_T}\sinh\left(\frac{w}{2}\frac{u-v}{v}\right)\exp\left[-\left(\frac{u-v}{v_T}\right)^2-\frac{1}{4}\left(\frac{w}{2}\frac{v_T}{v}\right)^2\right].$$

The relative permittivity of the surrounding dielectric is ε_r. This equation shows that gain (negative F) occurs whenever $u/v > 1$. This is in contrast to the zero-temperature case, where reduced scattering in low dimensions restricts the gain to a subset of this region.

Although T is an effective carrier temperature of the non-equilibrium 2DEG under bias, we proceed with the assumption that T = 300 K. The dependence of F on the phase velocity v, for frequency $\omega/2\pi$ = 1 THz, is shown in Figure 2-4. These curves are essentially unchanged over the entire frequency range 0.1-1 THz. The energy of drifting carriers can be transferred to a charge oscillation only when $(-F) > 0$, which occurs only for v/u between 0 and 1, i.e. the drift velocity must exceed the phase velocity *and* lie in the same direction. It is apparent that higher drift velocities also yield higher maximum growth rates. When $v > u$, on the other hand, the charge oscillation undergoes Landau damping, giving up energy to single-particle excitations of the electron gas.

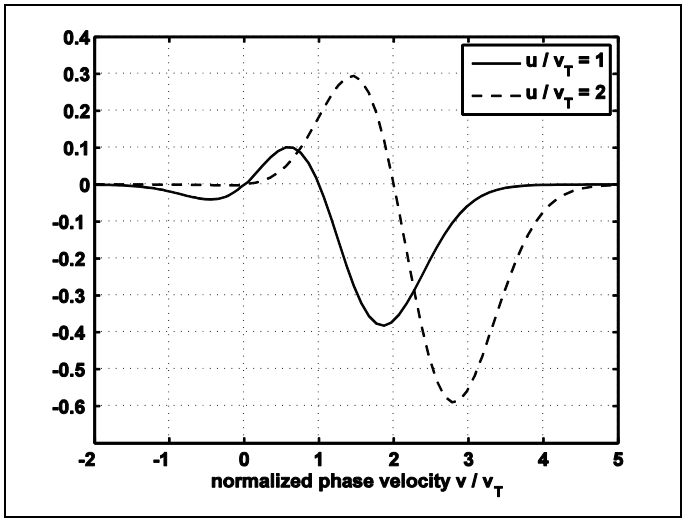

Figure 2-4. Dependence of the (negative) oscillator strength on the phase velocity v for 1 THz charge oscillations at room temperature. The curves are essentially unchanged over the range 0.1-1 THz.

Importantly, Landau damping also occurs if the charge oscillation moves in the direction opposite the drift velocity. In the context of a laser cavity, we must consider that the mode will reflect from the end-points of the device. If a mode grows in one direction, it will *lose* energy after reflection, once it begins to travel in the direction opposite the carrier drift. The above expression, then, should be considered a *forward* oscillator strength. In a cavity, it is appropriate to consider the "round-trip" oscillator strength, obtained by averaging the forward and backward directions:

$$F_{rt}(q,\omega) \equiv \frac{1}{2}[\, F(q,\omega) + F(-q,\omega)]\,.$$

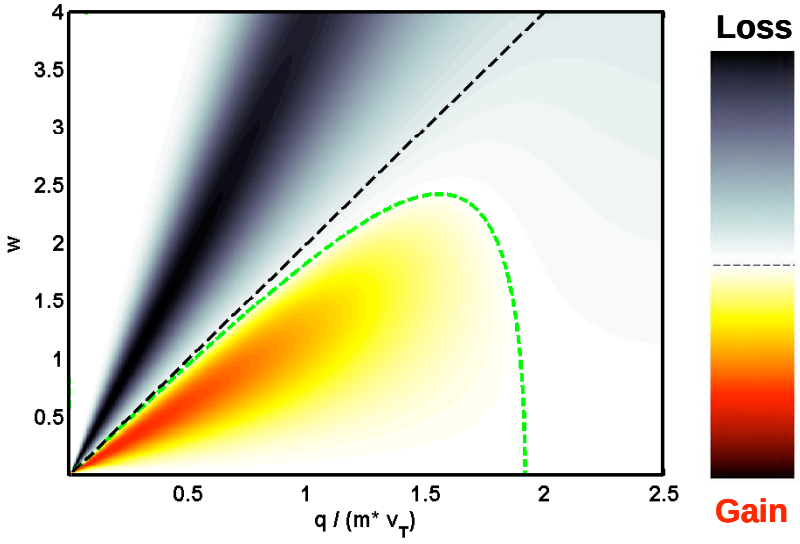

Figure 2-5. Round trip oscillator strength F_{rt} for drift velocity $u = v_T$, as a function of scaled frequency and wavevector. The loss region is shown in grayscale. The dashed green line denotes the boundary between loss and gain regions. The dashed black line denotes modes with phase velocity equal to the drift velocity.

This rate is shown for $u = v_T$ in Figure 2-5. Note that in the region $v < u$, the region below the dashed black line, there are modes for which the net growth is negative, i.e. the loss on the backward trip exceeds the gain on the forward trip. The boundary between loss and gain regions is shown as a green dashed line and satisfies the equation

$$\tanh\left(\frac{2\,u\,v}{v_T^2}\right)\tanh\left(\frac{w}{2}\frac{u}{v}\right)=\tanh\left(\frac{w}{2}\right).$$

One can show that this equation has solutions only when

$$u > v_c = v_T/\sqrt{2} = \sqrt{k_B T/m^*},$$

meaning that the drift velocity must exceed a critical velocity v_C in order for there to be *any* modes with positive round-trip gain. In other words, as the drift velocity decreases, the gain region in Figure 2-5. will shrink until it disappears entirely at $u = v_C$. The temperature dependence of v_C reflects the well-known fact that Landau damping increases with temperature.

We will later be interested in the long-wavelength regime, i.e. $q << m^* v_T$. Taking the $q \to 0$ limit with fixed phase velocity v,

$$F_{rt} \xrightarrow[q\to 0]{} -\frac{\sqrt{\pi}e^2}{2\varepsilon_0\hbar}\frac{n}{\varepsilon_r k_B T}\frac{v}{v_T}\left[u\sinh\left(\frac{2\,u\,v}{v_T^2}\right)-v\cosh\left(\frac{2\,u\,v}{v_T^2}\right)\right]\exp\left[-\left(\frac{u^2+v^2}{v_T^2}\right)\right]$$

For a given carrier velocity u, we define v_+ (v_-) to be the phase velocity at which this expression gives the maximum gain (loss). Figure 2-6 shows F_{rt} in the long-wavelength limit, with v_+ and v_- shown as solid black curves. To a reasonable approximation (which becomes excellent for $u >> v_C$),

$$v_\pm \approx u \mp v_C,$$

which is shown by dashed black lines. The plasma oscillation mode with the greatest amplification will have velocity $v_{+,}$ which evidently varies linearly with the drift velocity. This means that the lasing mode is frequency-tunable via the drift velocity. The round trip oscillator strength at the maximum gain velocity $v=v_{+}$ is approximately

$$F_{\max} \approx -\frac{\sqrt{\pi}e^2}{2\varepsilon_0\hbar}\frac{n}{\varepsilon_r k_B T}\frac{e^{-1/2}}{2\sqrt{2}}(u - v_C),$$

showing that maximum round trip gain is linear in both the drift velocity and carrier density.

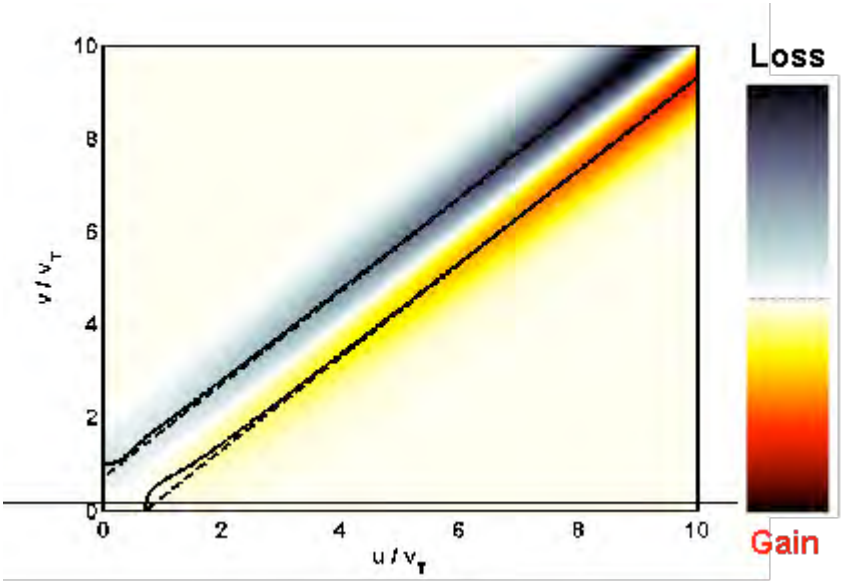

Figure 2-6. The long-wavelength limit of round-trip gain. The phase velocity v+ (v-) with maximum growth (loss) at fixed u is shown in black (solid curves), along with the approximate form (dashed curves).

2.4 Summary

In this section, we have shown how to analyze the mode gain available from drifting carriers in a solid state system. The crystalline lattice and quantum mechanical treatment introduce a number of effects not described by the plasma-physics approach of Section 1. The linear response of the system can be analyzed through the dielectric function, which can in principle be evaluated in the coupled electron-phonon system using diagrammatic methods of quantum statistical mechanics. A simplified approach is to use a phenomenological expression for the phonons and evaluate the electron contribution using the random phase approximation. The dielectric function can then be used to compute the growth or loss rate of plasma oscillations.

The concept of oscillator strength allows us to map the gain space for drifting carriers without reference to the phonons. This "gain map" then indicates how material and device characteristics can be chosen to optimize gain. For an electron gas, we find that at zero temperatures, phase space restrictions are present due to reduced dimensionality. In the classical limit, dimension is irrelevant to carrier kinematics but enters through the Coulomb interaction in Fourier space. Gain is possible whenever $u/v > 1$. However, in a laser cavity, reflections from the device endpoints mean that round trip gain is a more

appropriate figure of merit. We show that round trip gain occurs above a critical drift velocity v_C and provides maximum gain to modes with phase velocity $v = v_+ \approx u - v_c$. This means that the frequency of the lasing mode can be tuned via the drift current. Maximum gain is directly proportional to the carrier density and $u - v_c$.

3 Test case: metallic carbon nanotubes (mCNTs)

We now focus our attention on testing the feasibility of amplifying a 3P mode in a real material. Recall that by "3P" mode, we are referring specifically to a hybrid mode between phonons and electron plasma oscillations. Prerequisites for realizing this amplification are large electron drift velocities and strong electron-phonon coupling. In the previous section, we noted that the effective strength of the Coulomb interaction between carriers and phonons can be profoundly reduced by the details of the electron wavefunctions and normal oscillation modes of the lattice. Lattice symmetries play a key role in determining which electronic states and phonon modes are strongly coupled, making the results material-dependent. We identify metallic carbon nanotubes (mCNTs) as a high-mobility, low-dimensional material which is known to have strong electronic coupling to a longitudinal optical phonon in the THz regime. Below, we test the foregoing analysis against what is known experimentally about mCNTs.

3.1 Phonon emission at high bias

Metallic carbon nanotubes (mCNTs) are known to support high current densities, and electron-phonon coupling is believed to be strong between optical phonons and electrons in the lowest mCNT bands. Due to the chirality of the wavefunctions, the electronic states of the *d = 2* parent material, graphene, are robust against scattering from inhomogeneities which are large compared to the interatomic spacing[10]. This property suppresses backscattering from acoustic phonons while enhancing interaction with optical phonons. The bands closest to Dirac point in mCNTs inherit this property[11], leading to both high mobilities and strong electron coupling to optical phonons.

The transfer of electronic drift energy to phonons in mCNTs differs somewhat from the analysis of the previous sections because it involves *interband* transitions. Conduction and valence bands of an mCNT are linear and touch at two Dirac points in the Brillouin zone, labeled *K* and *K '*. Figure 3-1 illustrates the occupation of electronic states of an mCNT under bias (a) near one of the Dirac points. The bias pushes electrons (holes) into conduction (valence) band states with current in the bias direction. Phonon emis-

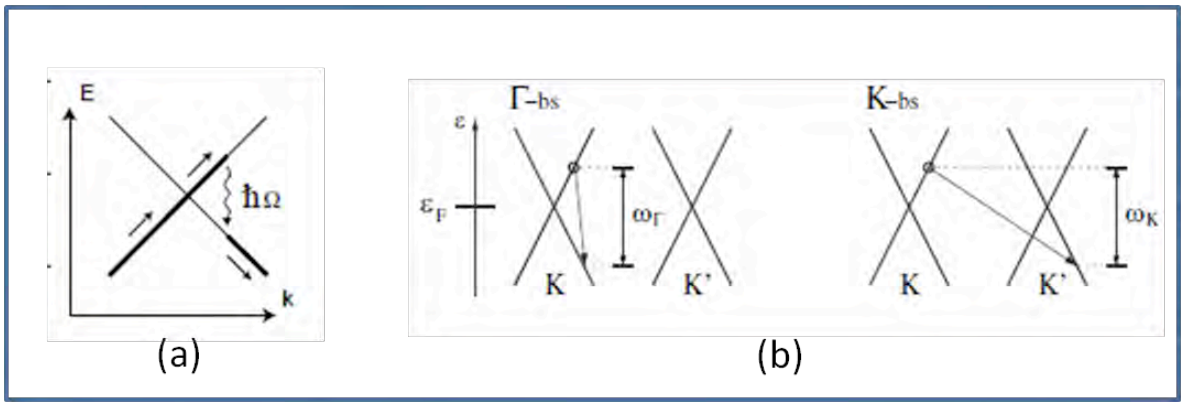

Figure 3-1. Electronic states in an mCNT under bias. a) Electrons (holes) fill conduction (valence) band states whose current lies in the bias direction. b) Different phonon modes are excited depending on whether the electron and hole are located near the same Dirac point.

sion can occur when there is an available electron transition with energy equal to the phonon energy. This is a very different criterion than the $u > v$ requirement of the intraband, quadratic-dispersion case analyzed earlier. Phonon modes Γ and K are excited (b) depending on whether the electron transition occurs between different Dirac points.[12]

Experimentally, there is ample evidence of a long mean free path for electrons near the Fermi level[13]. However, transport experiments with low-resistance contacts[14] show that energetic electrons and holes are strongly scattered. The conductance reaches a maximum at about 100 mV, above which voltage it drops dramatically. Bandstructure suggests that the exhaustion of states in the lowest band should not occur until a much higher voltage of about 2.9 V. The current saturation behavior (see Figure 3-2) is instead consistent with the relaxation of excited carriers by the emission of a mode with energy about 0.16 eV, which coincides with the emission threshold for optical phonons.

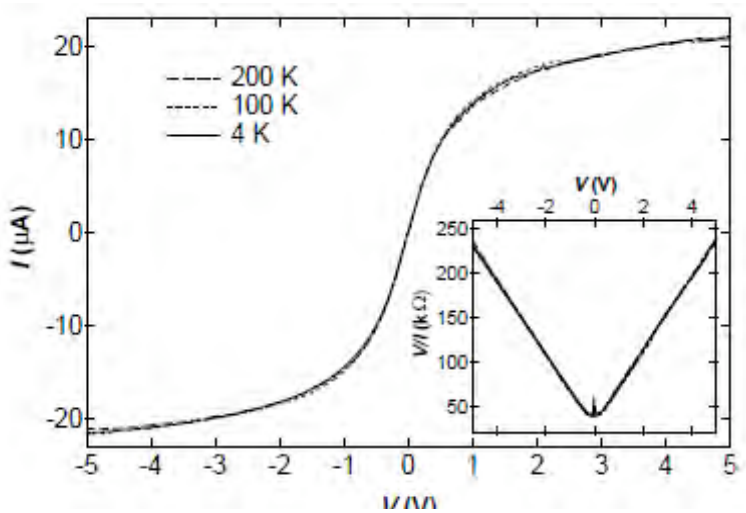

Figure 3-2. I-V characteristic of an mCNT [from Yao, Kane, Dekker, Physical Review Letters 84, 2941 (2000)]. The onset of current saturation begins at about 100 mV, as evidenced by resistance V/I that increases linearly with voltage (inset).

The high-bias emission of phonons in mCNTs has been studied theoretically by several authors[15]. Figure 3-3 shows the theoretical electronic scattering rate from phonons as a function of transition energy, computed for a type (25, 0) nanotube. Scattering from K_{LO} and Γ_{LO} optical phonon branches is considerably stronger than for acoustic and radial modes. This explains the high conductance observed below the K_{LO} emission threshold of about 0.18 eV and the current saturation above. Note that the scattering rate is strongly peaked near the emission threshold for each band. This is due to a diverging density of phonon states near the threshold and is a generic feature of one-dimensional systems. We generally expect emission of any mode in one dimension to appear strongly and abruptly at the emission threshold[16].

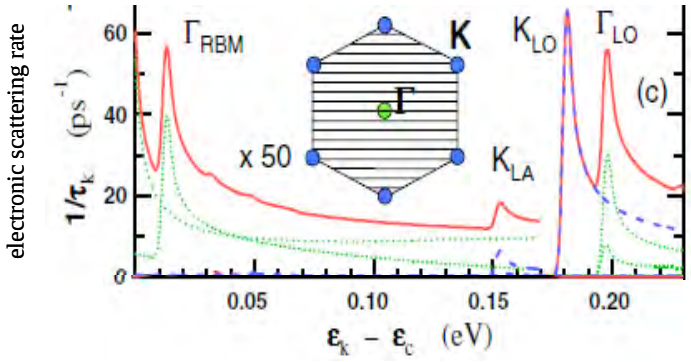

Figure 3-3. Electronic scattering rate from phonons as a function of transition energy, computed for a type (25,0) nanotube. Scattering rates below 0.17 eV are magnified by a factor of 50. Scattering from K_{LO} and Γ_{LO} optical phonon branches is considerably stronger than for acoustic and radial modes.

3.2 Why mCNTs do not radiate via an amplified 3P mode

We have seen that mCNTs have a built-in mechanism for transferring energy from the electronic current to an LO phonon mode. If the 3P mode amplification idea is valid, we should expect mCNTs under high bias to radiate coherently at about 40 THz, corresponding to the emission threshold energy of the K_{LO} phonon. Although mCNTs appear to have the right properties for the amplification of a 3P mode under high bias, we know of no such experimental findings in the literature. In the following, we explain why this is the case and discuss the implications for 3P mode amplification in real materials.

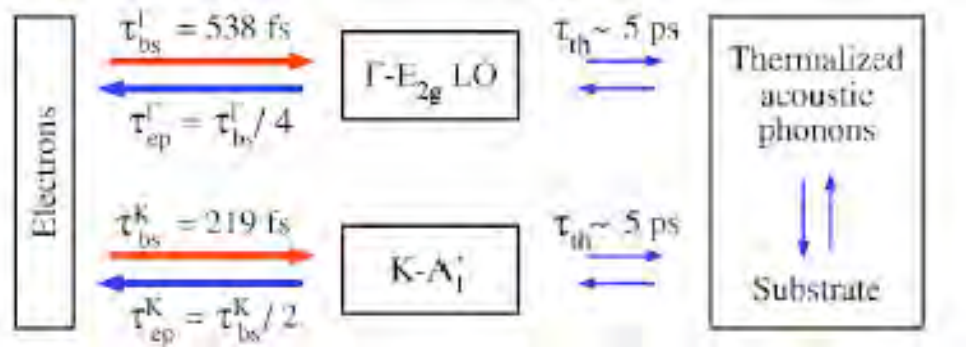

Figure 3-4. Time constants for the scattering of electrons by optical phonons and the subsequent decay of optical phonons into acoustic phonons [from M. Lazzeri and F. Mauri, Phys. Rev. B 73, 165419 (2006)].

Calculations of electron-phonon and phonon-phonon scattering times have been carried out for mCNTs and are illustrated in Figure 3-4. Phonon emission from hot electrons occurs on a sub-picosecond time-scale, after which LO phonons undergo anharmonic decay into acoustic phonons. The timescale for this decay is much longer, about 5 ps, so we would still naïvely expect net amplification. On the other hand, optical phonons are essentially nondispersing and thus have very low *group* velocity. An emitted phonon therefore travels a negligible distance down the nanotube before it decays. As a result, injected carriers lose their energy to *incoherent* optical phonons within a very short distance from the contacts. These decay into acoustic phonons, with the end result that the drift energy is converted into heat. Away from the contacts, the electron population is near equilibrium, and no mode gain is possible.

Amplification of the 3P mode along the length of the nanotube also requires that the associated electromagnetic fields be strongly confined to the tube[*]. This can occur if the *phase* velocity of the mode is much slower than the vacuum speed of light. Fast modes, on the other hand, will "leak" radiation into free space. The slow mode criterion is met by the K_{LO} phonon (because of the large momentum transfer associated with electron scattering between the Dirac points) but not the Γ_{LO} mode. Although K_{LO} emission should dominate since it has a lower threshold and stronger coupling to electrons, the excitation of the Γ_{LO} mode leads to significant radiative losses orthogonal to the tube. In principle, this could be mitigated by placing the nanotube in a lasing cavity.

While mCNTs do not appear to be viable for directly generating coherent THz radiation, the sudden onset of electron scattering due to optical phonon emission may be exploited in a THz relaxation oscillator[17].

3.3 Conclusions

We conclude that three factors explain the apparent lack of 3P mode amplification in mCNTs. The anharmonic decay of optical phonons limits the coherence time of the 3P mode to about 5 ps. Due to the low group velocity, the mode fails to propagate away from the contacts before this decay. The high phase velocity of one of the excited phonon modes leads to radiative losses orthogonal to the tube.

We expect some of these difficulties to be generic to realizing amplification of a phonon-based hybrid mode in semiconductor-based nanostructures. THz-frequency phonons lie in optical bands, which invariably have low group velocities and undergo anharmonic decay into acoustic phonons. We thus expect the electronic drift energy to be converted to heat close to the device contacts. If the phonon couples to direct interband electronic transitions, the associated mode will be fast and thus leak radiation transverse to the (low-dimensional) nanostructure. Indirect transitions may excite modes that are sufficiently slow to remain strongly confined to the nanostructure.

Realizing amplification of a 3P mode will likely require some engineering control over phonon properties. Unfortunately, low-dimensional nanostructures have phonon spectra significantly more complicated than in bulk. The reduced spatial extent along confining directions leads to folding of the Brillouin zone and the attendant multiplication of dispersion branches. This is illustrated in Figure 3-5, which juxtaposes a) the *d = 1* phonon spectrum of a type (10,10) carbon nanotube with that of b) graphene, its *d = 2* parent crystal[18]. The former has 66 distinct branches in the spectrum as opposed to 6 in the latter. For semiconductors in general, engineering the size of the nanostructure in directions transverse to the electron drift current can in principle be used to control the spacing between these additional branches. Additional manipulation of the spectrum could conceivably be accomplished by squeezing the lattice at high pressure. On the other hand, the spectrum is probably the only aspect of phonons amenable to engineering control. Electron-phonon couplings are difficult to predict or measure accurately, let alone control, and it is difficult to imagine a way to solve the problem of anharmonic phonon decay.

We conclude that phonons will not be part of a realizable THz laser concept based on the hybrid mode idea. In the next section, we consider an alternative to phonons based on periodic metal films.

[*] This requirement can be avoided in a nanotube array, in which radiation orthogonal to a tube can be amplified by neighboring tubes.

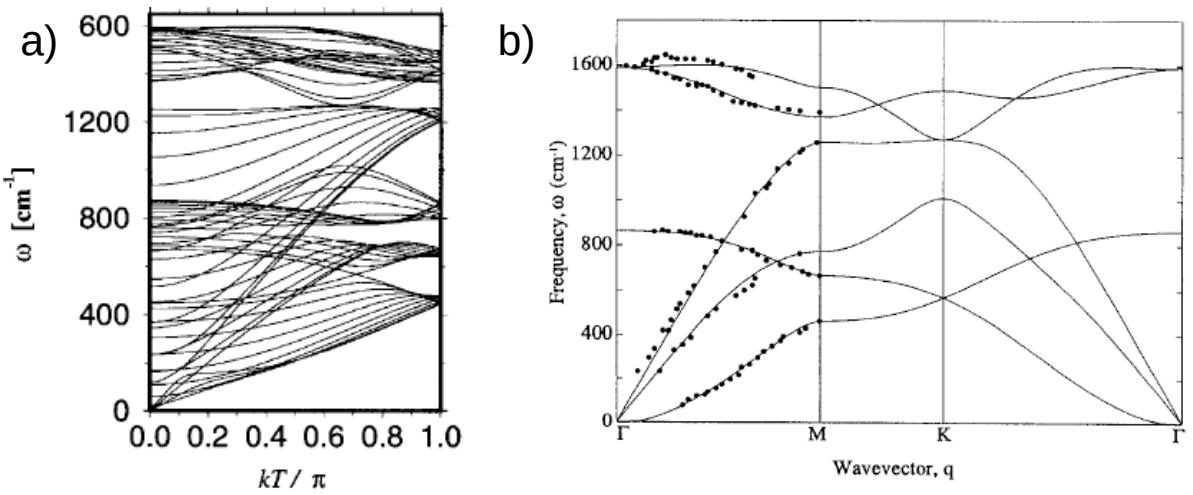

Figure 3-5 Calculated phonon spectra for a) a (10,10) carbon nanotube and b) the parent crystal graphene, from M. S. Dresselhaus and P. C. Klund, Advances in Physics, 2000, Vol. 49, No. 6, 705-814.

4 Device proposal based on periodic metal films (PMFs)

4.1 Concept and rationale

The role of phonons in the 3P mode is to provide a charged system which exchanges energy with streaming charged carriers and radiative photon modes. Given the shortcomings of phonons discussed in the previous section and the considerable challenge of trying to find, predict, or engineer a crystalline system with suitable phonon characteristics, we consider whether the role of phonons can be played by a different charged system. We take the approach that the fastest route to a realizable THz source based on the hybrid mode idea is to draw upon on existing mature nanofabrication technologies and engineering concepts. The main physical requirement leading to mode amplification is that the streaming carrier velocity exceed the phase velocity of charge oscillations. We need, then, technologies that can provide both large carrier velocities and slow phase velocity.

While lattice ions and electrons in crystals occupy the same volume in space, the hybrid mode idea does not necessarily require that the two charge systems overlap. The coupling of longitudinal waves in the two charge systems is due to the electrostatic Coulomb interaction between moving charges. As a result, the two systems can remain strongly coupled through electromagnetic fields as long as their separation is comparable to or less than the decay length of the relevant evanescent wave. We will later discuss why such separation may even be preferable. This means that we can solve the technological problems of attaining high carrier velocity in one system and slow phase velocity in a second system and then bring the systems into close proximity. This approach offers a tremendous simplification, in terms of fabrication, compared to approaches in which carriers move directly through slow-wave structures.

For fast carriers, high electron mobility transistors (HEMTs) based on wide band gap semiconductor heterostructures offer high saturation velocities at room temperature and above. These devices consist of two semiconductor slabs, differently doped, trapping a high-mobility two-dimensional electron gas (2DEG) at the interface. Some possible choices for the semiconductor are GaN and various polymorphs of SiC. In particular, SiC-4H combines high saturation velocity with high thermal conductivity, which helps to mitigate ohmic heating. The HEMT gates also allow in principle for the areal density of electrons in the 2DEG to be changed in situ, offering another means of continuous tuning the laser during operation, in addition to the drift current. Fabrication technologies for HEMTs are well-developed and include molecular beam epitaxy (MBE) and various etching methods.

Figure 4-1. Two-dimensional device with two charge systems in adjacent layers. Streaming electrons are provided by the 2DEG, while a PMF provides slow modes that couple to the 2DEG via evanescent fields.

Periodic metal structures have long been used at microwave and radio frequencies to engineer slow waves in cavities and traveling wave tubes. The backward wave oscillator (BWO) is a device which uses the interaction between a periodic metal structure and an electron beam to generate coherent, frequency-tunable radiation. Our device concept is, in fact, a solid-state, micro-scale BWO. We expect the detailed design of such a device to leverage the body of engineering knowledge developed for BWOs, with careful allowance for new phenomena due to the change in scale.

With a HEMT under bias providing a two-dimensional sheet of streaming carriers, we are led to the notion of layered device with the two charge systems in adjacent layers, as illustrated in Figure 4-1. This means that the second charge system, which provides the slow wave, should also be two-dimensional. A variety of techniques have been developed in the last decade for creating periodic metal films (PMFs). These films come in various forms, such as metal films with periodic hole arrays[19] or groove arrays[20] or alternatively periodic arrays of metallic nanospheres and nanodisks[21]. PMFs and related metal structures have drawn considerable interest in the last decade due to some exotic optical properties such as extraordinary selective transmission, sub-wavelength focusing, and extremely large local fields.

Detailed engineering of slow waves in PMFs is possible by controlling the periodicity of the array, the shape of holes/grooves/particles, the film thickness, and the dielectric properties of adjacent device layers. High-conductivity metal such as Ag or Au is typically chosen to minimize ohmic losses. The metal may also be chosen so that the skin depth is close to the film thickness or the size of metal particles, leading to exotic electromagnetic phenomena which could be exploited in device design.

Our proposal is flexible as to the selection of a particular kind of PMF, but for concreteness we discuss metal films perforated with an array of holes. These films can be fabricated with sub-micron hole spacing and are known to support surface waves known as spoof surface plasmons (SSPs). A typical analysis[22] regards the holes as short waveguides couple surface fields on either side of the film, as illustrated in Figure 4-2. At long wavelengths, the mode velocity is close to the speed of light, meaning that SSPs tend to be poorly confined.

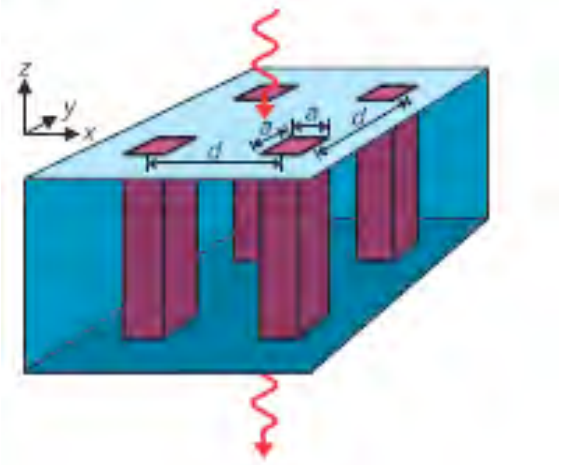

Figure 4-2. The holes in a metal film may be regarded as waveguides coupling the surface fields on either side of the film. (from J. B. Pendry et al., Science, Vol. 305, 6 August 2004)

However, recent experimental and theoretical work[23] has shown that when the metal film is adjacent to a dielectric slab, as shown in Figure 4-3 (left), SSP modes hybridize with guided wave (GW) modes of the dielectric, leading to slow waves whose fields are strongly confined to the dielectric. The properties of this SSP-GW mode, including its phase and group velocity, can be engineered via the slab thickness, dielectric constant, and metal film properties. We anticipate that such modes will appear for other PMFs placed adjacent to a dielectric slab. Since a slow wave cannot propagate in free space, it undergoes total reflection at the boundaries of the slab. Thus the slab can serve as a high-Q laser cavity for the slow wave. Later in this section, we will address the issue of getting radiation out of the device, i.e. coupling the slow wave to free-space radiation. In our notional layered HEMT/PMF device shown in Figure 4-1, the HEMT itself provides the dielectric slab required to confine the slow mode. Note that in Figure 4-3

(right), the SSP-GW mode can penetrate far into the dielectric and thus should couple strongly to the 2DEG in our device.

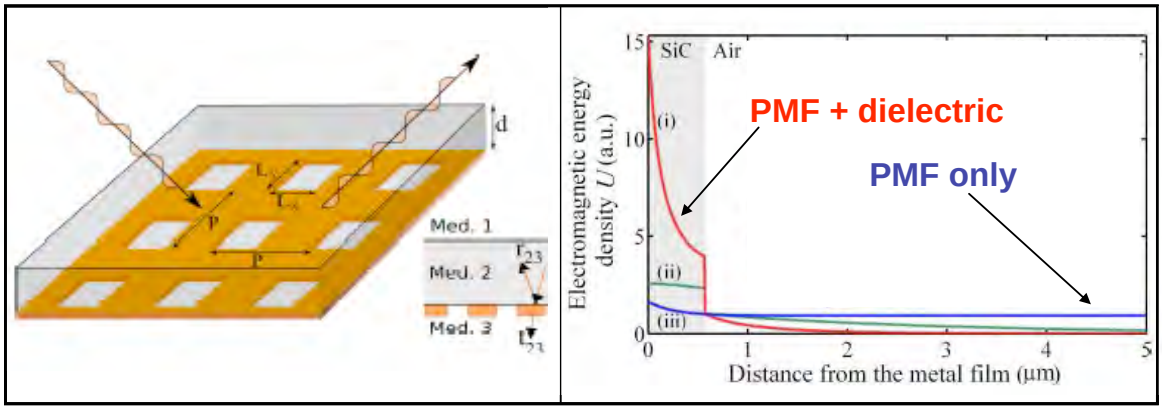

Figure 4-3. When a metal film with periodic hole array is placed adjacent to a dielectric slab (left), SSPs hybridize with the guided wave modes of the slab to produce strongly confined slow modes. The electromagnetic energy density (right) shows that the hybrid wave (red) is much more strongly confined that the SSP of the metal film alone (blue) [Moussavi et. al. Phys. Rev. Lett. ***105****, 176803 (2010)]*

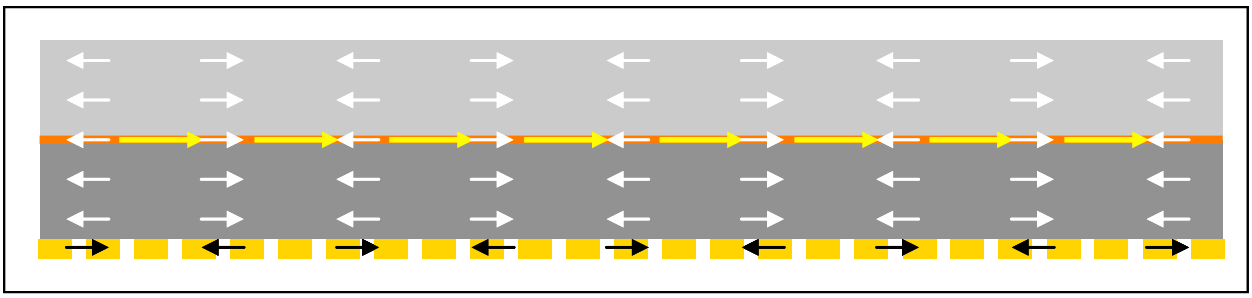

Figure 4-4. A schematic view of charge velocities (black) and longitudinal electric fields (white) of a HEMT-PMT device during operation.

Figure 4-4 provides a schematic snapshot of charge velocities (black) and longitudinal electric fields (white) of the lasing mode. The carriers of the 2DEG drift to the right while the charges in the PMF oscillate. The electric fields of the slow mode are strongly confined to the dielectric slab and undergo essentially perfect reflection at its endpoints. Thus we expect device performance to be limited not by radiation leakage, but by power dissipation in the device materials, which has three components. Power efficiency will likely be limited by the dc power required to drive the drift current in the HEMT. This in turn generates ohmic heating, which both reduces electron mobility and increases the critical drift velocity required for round-trip mode amplification. An efficient heat sink and low sheet resistance will be critical to the design of a practical device. The effective Q of the cavity, on the other hand, will be li-

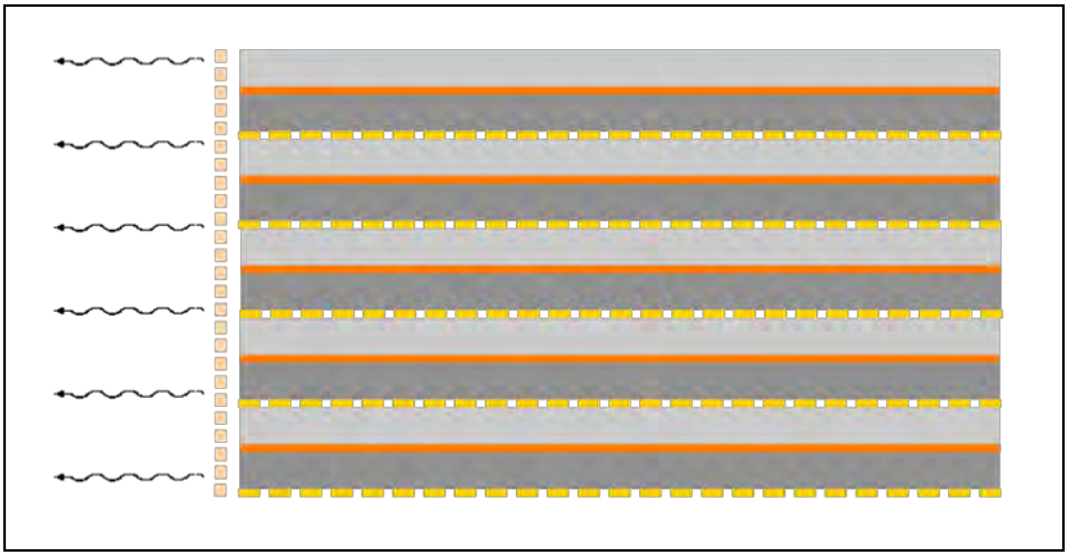

Figure 4-5. The basic device unit can be repeated to obtain high power densities. An additional PMF (left) serves to couple the confined mode to free-space radiation, as well as improve collimation, coherence, and bandwidth.

mited by the ohmic losses of the oscillating charges in the PMF and the absorption or scattering of radiation by the dielectric. The former can be minimized by choosing a high-conductivity metal such as Ag or Au in the PMF. It is possible that the type of PMF (e.g. metal particles vs. hole arrays) can be chosen to minimize these losses. We expect direct absorption in the dielectric to be negligible at THz frequencies, but the scattering of electromagnetic waves from crystalline defects may be important in a heavily doped layer of the HEMT.

Finally, we note that in a practical device, high power density can be achieved by repeating this basic device unit, as illustrated in Figure 4-5. The structure on the left is an additional PMF that couples the lasing mode to free-space radiation. Its frequency- and angle- dependent reflectivity can be engineered to provide selective feedback, thereby collimating the output, improving interlayer coherence, and reducing the bandwidth. Such a PMF has recently been designed to improve the performance characteristics of a quantum cascade laser[24].

4.2 Amplification of slow modes in the HEMT-PMF system

Below, we give an idea of how mode growth occurs through evanescent coupling of the 2DEG to the PMF. We consider a simplified system consisting of an infinite 2DEG and PMF separated by an ideal dielectric with constant μ, ε. We take the PMF to be periodic only in the x direction (the direction of the drift velocity u) and uniform in the transverse (y) direction, as would be the case in an array of metal

wires or grooves. The device layers are stacked in the z direction. The basic picture is shown in Figure 4-6.

We first consider the gain conditions for the 2DEG. The 2DEG can be treated classically at room temperature and above. We would like to take advantage of the high Q of the lasing cavity and consider the round trip net growth under multiple reflections. The thermal length scale $h/(m^* v_T)$ is roughly 10 nm, so we may evaluate the oscillator strength in the long-wavelength limit $q \to 0$. The analysis of Section 2.3.2 shows that in this regime, the round-trip gain is greatest for modes with phase velocity $v \approx u - v_C$, where u is the 2DEG drift velocity and $v_C = (k_B T/m^*)^{1/2}$.

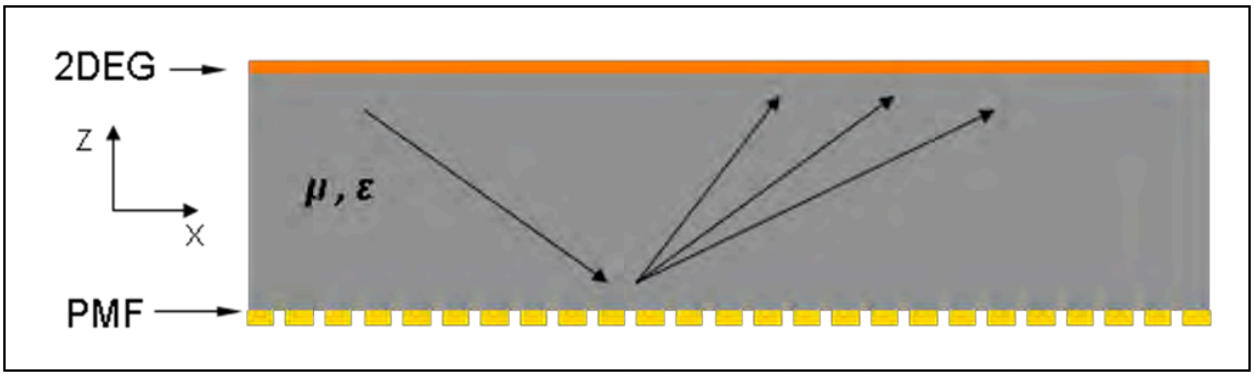

Figure 4-6. An wave incident on the PMF is scattered into a series of waves with different phase velocities v_m. The evanescent decay of these waves away from the PMF is fastest for slow-moving waves. Amplification of waves with $u/v_m > 1$ occurs upon reflection from the 2DEG and is maximized for $v_m \approx u - v_C$.

The lasing mode is TM-polarized, comprised of plane waves in the dielectric with electric fields of the form

$$\vec{E} = e^{j(\pm kz + qx - \omega t)}(-q\hat{z} \pm k\hat{x})/(\sqrt{\mu\varepsilon}\,\omega)$$

where q and ω are real and $k=(\mu\varepsilon\omega^2 - q^2)^{1/2}$. The periodicity L of the PMF implies that the guided-wave eigenmodes in the dielectric consist of a fundamental wave at $q = q_0$ admixed with a series of diffracted waves at $q = q_m \equiv q_0 + 2\pi m/L$. "Slow" waves have phase velocity $v_m = \omega / q_m$ slower than the speed of light in the dielectric $c = (\mu\varepsilon)^{-1/2}$, meaning that $k_m=(\mu\varepsilon\omega^2 - q_m^2)^{1/2}$ is imaginary. These waves decay in the z (or $-z$) direction, with shorter decay length for slower partial waves. Very slow waves with $v_m << c$ also have $|k_m| \approx |q_m|$, so that the x and z components of the electric field have comparable magnitude. For $q_0 L << 1$, the phase velocity of the lowest eigenmodes will be comparable to the speed of light in the dielectric. Thus for large ε, *all* partial waves are very slow relative to light in *free* space and thus are strongly confined to the dielectric.

The dispersion relation $\omega(q_0)$ for the eigenmodes can be computed from the reflection coefficients for the 2DEG and PMF surfaces. A wave incident on the PMF scatters into a series of outgoing waves with wavevectors that differ by integer multiples of $2\pi / L$. The PMF is thus characterized by a *matrix*-valued reflection coefficient $r_{mn}(q_0,\omega)$ which relates the q_n component of the outgoing wave to the q_m component of the incoming wave. Since the 2DEG is uniform in both x and y directions, its reflection matrix is diagonal, but for waves slower than the drift velocity ($u/v_m > 1$) the modulus of the reflection coefficient is greater than 1. This amplified reflection can occur because the dielectric response of the drifting 2DEG satisfies

$$\omega \mathrm{Im}\, \varepsilon_{2\mathrm{DEG}}(q_m, \omega) < 0 .$$

We propose choosing the PMF period L to maximize the round-trip gain for the $m = \pm 1$ partial waves. This is accomplished by setting the phase velocities $|v_{\pm 1}| \approx u - v_C$, implying the following "rule of thumb" for the lasing frequency ν :

$$\nu L \approx \mathrm{u} - \mathrm{v}_C .$$

The lasing frequency can therefore by tuned by the drift current, as is true for analogous microwave backward wave oscillator (BWO) devices. Since achievable drift velocities are much slower than the speed of light in the dielectric, the electric fields of the $m = \pm 1$ partial waves will have a significant component parallel to the plane of the 2DEG and thus couple strongly to electron oscillations.

The dielectric thickness t can be chosen so as to render the higher partial waves ($|m| > 1$) unimportant. As $|m|$ increases, a partial wave decays in the z direction by a factor of approximately $e^{-2\pi |m| (t/L)}$ between the 2DEG and the PMF. Choosing t to be larger than or comparable to L suppresses the exchange of energy between the 2DEG and PMF through the higher partial waves. On the other hand, t should not be so large as to overly suppress the $|m| = 1$ waves.

In addition to being readily engineered, the PMF addresses the weaknesses of phonons identified in Section 3, namely high phase velocity, low group velocity, and significant damping (due to anharmonic phonon decay) over one period of oscillation. The reflection of partial waves from the PMF creates the slow phase velocities necessary for both amplification and confinement within the dielectric. The *group* velocity of the eigenmodes, on the other hand, is expected to be close to the speed of light in the dielectric. The attenuation length associated with ohmic dissipation in a high-conductivity PMF is much larger than its periodicity L, which, as we show below, is at the sub-micron scale.

4.3 Realistic device parameters

In this section, we propose a set of device parameters for achieving amplification in the range 0.1-10 THz. These parameters are accessible with existing fabrication technology. We comment on anticipated performance characteristics of the device and indicate what additional modeling work is needed to make precise quantitative estimates.

The key device requirements are high electron mobility and high maximum carrier velocity at room temperature and above. Interest in high-power applications has lead to the development of HEMTs with these properties based on wide band gap semiconductors. We will base our estimates on 4H-SiC, a typical semiconductor in such HEMTs. Assuming $m^* = 0.4\, m_0$, the critical velocity for round trip gain at 300 K is

$$\mathrm{v}_\mathrm{c} = \sqrt{k_B T / m^*} \approx 1.1 \times 10^7 \text{ cm/s} .$$

Recent high-power HEMTs have achieved room-temperature saturation velocities as high as 2.7×10^7 cm/s so that round-trip gain should be possible in currently available HEMT devices at room temperature and above. We assume that our device can achieve drift velocities as high as $2\, v_C$, so the phase velocity $v \approx u\text{-}v_C$ of the lasing mode can be as high as v_C. For a maximum lasing frequency of 1 THz, our "rule of thumb" implies a PMF periodicity of $L = 0.1$ µm, with smaller periodicity required for higher frequencies. Nanohole arrays in Ag films are typically fabricated in the range 0.5-1.0 µm, implying a 0.2 THz maximum lasing frequency. Alternatively, block copolymer templates can be used to self-assemble

two-dimensional Ag nanoparticle arrays[25] with L = 10-100 nm, raising the maximum lasing frequency to 10 THz.

Initial work on the 3P mode showed that for drift velocities comparable to v_C, the mode growth rate is comparable to the mode frequency, i.e. growth by a factor comparable to e occurs per wavelength of oscillation. The ohmic loss rate per wavelength in the dielectric and PMF is essentially negligible, so that the lasing mode should achieve large net amplification during one round-trip. A quantitative estimate of the output power and efficiency requires an understanding of the gain saturation and detailed modeling of the inhomogeneous carrier and photon populations. This is left for future work. For the device to operate efficiently, the radiation power must be comparable to the dissipation implied by the resistance of the 2DEG. This requires that the mode intensity at gain saturation is large enough that the stimulated emission time for an electron in the 2DEG be comparable to the collision time, which for present parameters is of order 1 ps. A typical sheet resistance R_s= 250 Ω and electron density n = 10^{12} cm^{-2} implies that at the lasing threshold the dc power required *per device layer* is about

$$P_{dc} = (env_C)^2 R_s \approx 8 \text{ Watt mm}^{-2}.$$

Since P_{dc} is quadratic in n, this can be reduced considerably by operating at a lower carrier density. This comes at the expense of the growth rate, however, and the optimization of n requires additional, application-specific modeling.

Parameters for a realistic device are summarized in Table 4.1. We conclude that mode growth rates comparable to the mode frequency are possible in our device at room temperature. Cooling may be necessary mitigate heating of the drifting carriers, but this requirement is manageable and a considerable improvement over quantum cascade lasers, which require cryogenic operating temperatures. We anticipate that the dielectric will serve as a high-Q lasing cavity, and we are optimistic that mode intensities can be made sufficient high for efficient laser operation. Additional modeling is required to optimize the carrier density and obtain quantitative estimates for output power and efficiency.

Table 4.1 Assumed parameters for a realistic device, based on 4H-SiC properties, currently available HEMTs for high power applications, and accessible PMF periodicities.

Component	***Property***	***Symbol***	***Value***
HEMT			
	carrier effective mass	m^*/m_0	0.4
	critical velocity @ 300 K	v_C	1.1 x 10^7 cm/s
	saturation velocity at 300 K	v_s	2.7 x 10^7 cm / s
	maximum drift velocity	u	2 v_c = 2.2 x 10^7 cm/s
	2DEG mobility at 300 K	μ_e	2 x 10^3 cm^2 / V s
	sheet resistance	R_s	250 Ω
	area density of carriers	n	10^{12} cm^{-2}
PMF			
	period	L	10 nm - 1 μm
	operating frequency	ν	< 10 THz

4.4 Path to a Prototype

Although we have useful theoretical results for the oscillator strength of the 2DEG, computing the growth rate requires a quantitative analysis of a single-layer device along the lines of Section 4.2. Using a semi-analytic simplified model for partial wave reflection, the goal would be to establish top-level requirements for the PMF, for example a cutoff frequency for surface modes and surface impedance. We would then be in a position to assess which type of PMF most promising. This effort would also address the effect of dielectric thickness on the strength of coupling between the 2DEG and the PMF.

With top-level parameters for the PMF established, a "custom" PMF can be designed using commercial electromagnetic finite-element analysis software, such as COMSOL. The out-coupling PMF of a multi-layer device could be designed using the same approach. If a HEMT-PMF system can be fabricated with *tunable* carrier density over several orders of magnitude, we would, at this point, be in a position to design a device. Predicting gain saturation, power output, bandwidth, and efficiency of the device requires solving a separate transport model to find self-consistent carrier and photon distributions in a finite-size device under lasing conditions. Such a model would also help to optimize the carrier density in a fixed-density device. The existing literature on backward-wave oscillators should provide a template for this analysis.

An initial device fabrication effort would focus on a single-layer device. Although the PMF and HEMT components are apparently feasible, bringing them together may require innovative fabrication methods or collaboration between laboratories, depending on the type of PMF. Analyzing device performance also requires THz detection capability. Since the lasing mode decays within a micron or less of the surface of the dielectric, a conducting antenna structure (preferably with tunable transmission coefficient) must be introduced in order to detect the lasing mode.

5 Summary

This report presents and analyzes a solid-state device concept for compact, dc-driven, room-temperature generation of coherent THz radiation. The advent of low-dimensional high-electron-mobility devices (HEMT) suggests that a micro-scale, solid-state analog of vacuum tube electron-beam microwave sources may be feasible. The project began by analyzing the two-stream instability between electrons and optical phonons in semiconductors. This effort established conditions for the amplification of the resulting hybrid plasmon-phonon-polariton (3P) mode. The analysis showed that the growth rate becomes comparable to the mode frequency when the average carrier velocity exceeds the thermal spread.

A succeeding project phase addressed shortcomings in the earlier plasma-physics-based analysis. Tools from condensed matter physics generalized the first analysis approach to handle low dimensionality, low temperatures, and high carrier densities. The oscillator strength concept was used to generate "gain maps" to identify areas of the phase space offering optimal growth conditions. Low dimensionality and quantum statistics significantly affect the distribution of gain in phase space. In the classical limit, appropriate at room temperature, we found that carrier drift must exceed a critical velocity v_C, in order for the lasing mode to have positive round-trip gain.

Metallic carbon nanotubes (mCNTs) were then analyzed as a test case for the 3P mode idea. Experimental evidence points to the strong emission of optical phonons at high bias. We identified three reasons preventing the development of a 3P mode which is amplified as it propagates down the tube. The optical phonons decay into acoustic phonons on timescales of order 5 ps. The group velocity is sufficiently slow that phonons decay close to the contacts, and the nanotube cannot sustain a non-equilibrium carrier population down its length. The phase velocity of the phonons is large, so that radiation fields necessary to the 3P mode escape transverse to the tube. We observe that anharmonic decay, low group velocity, and high phase velocity are generic features of optical phonons. These shortcomings, as well as the difficulties of engineering phonon properties, indicate that a practical device of this type cannot be based on a 3P mode.

Project focus was then returned to the more general two-stream instability and consideration of surface waves in a periodic metal film (PMF) playing the role of phonons in the two-stream instability. Using this new field-modifying element, we came up with a HEMT-PMF device design in which the streaming electrons of the HEMT excite surface waves of the PMF through exchange of evanescent waves. This scheme not only addresses the shortcomings of phonons; the HEMT itself becomes a high-Q cavity for the lasing mode. We showed that existing HEMT devices attain drift velocities leading to growth rates comparable to the mode frequency at room temperature. The lasing frequency is tunable via the drift velocity and can attain a maximum of between 0.2 and 10 THz, depending on the type of PMF used. Losses are dominated by the ohmic dissipation of drifting electrons, which can be reduced by lowering the carrier density, although at the expense of gain.

Subsequent work on this concept should start with quantitative estimates of power output and efficiency, which will require modeling of the carrier distribution during laser (i.e., resonant cavity) operation; theoretical treatment of backward wave oscillators can serve as a starting point. Fabrication of a test device requires additional modeling for the design of the PMF. Combining the HEMT and PMF technologies and evaluating a prototype device may require the collaboration of several research groups experienced in the relevant disciplines.

6 References

[1] W. Knap, J. Lusakowski, T. Parenty, S. Bollaert, A. Cappy, V. V. Popov and M. S. Shur, "*THz emission by plasma waves in 60nm gate HEMTs*", Applied Phys. Lett. **84** 2331 (2004), Phys. Rev. Lett. **71**, 2465 (1993)
[2] N. Krall and A. Trivelpiece, Principles of Plasma Physics (1973)
[3] S. Riyopoulos, *Physics of Plasmas* **12**, 070704 (2005)
[4] S. Riyopoulos, *Physics of Plasmas* **16**, 033103 (2009)
[5] S. Riyopoulos, unpublished
[6] A. V. Kuznetsov and C. J. Stanton, *Phys. Rev. Lett.* **73**, 3243 (1994)
[7] J. Rammer, Quantum Field Theory of Non-equilibrium States (2007) ; S. Fujita, Introduction to Non-Equilibrium Quantum Statistical Mechanics (1966)
[8] G. D. Mahan, Many-Particle Physics (1980),; A. Fetter and J. Walecka, Quantum Theory of Many-Body Systems (2003); A. Abrikosov, L. Gorkov, Dzyaloshinski, Methods of Quantum Field Theory in Statistical Physics (1975)

[9] Jackson, Classical Electrodynamics (1999)
[10] A.H. Castro-Neto, F. Guinea, N.M.R. Peres, K.S. Novoselov, A.K. Geim, *Reviews of Modern Physics* **81**, 109-162 (2009)
[11] T. Ando, T. Nakanishi, and R. Saito, *J. Phys. Soc. Jpn*. **67**, 1704 (1997)
[12] M. Lazzeri, S. Piscanec, F. Mauri, A.C. Ferrari, J. Robertson, *Phys. Rev. Lett.* **95**, 236802 (2005)
[13] S.J. Tans el al., *Nature* **386**, 474 (1997); P.L. McEuen et. al., *Phys. Rev. Lett.***83**, 5098 (1999)
[14] Z. Yao, C. Kane, C. Dekker, *Phys. Rev. Lett.* **84**, 2941 (2000); Park et. al. *Nano Letters* **4**, No. 3, 517-520 (2004)
[15] V. Perebeinos, J. Tersoff, P. Avouris, *Phys. Rev. Lett.***94**, 086802 (2005); M. Lazzeri and F. Mauri, *Phys Rev. B* **73**, 165419 (2006); M. Lazzeri, S. Piscanec, F. Mauri, A.C. Ferrari, J. Robertson, *Phys. Rev. Lett.* **95**, 236802 (2005)
[16] E.H. Hwang, B. Hu, S. Das Sarma, *Phys. Rev. B* **54**, 4996 (1996)
[17] G. Pennington and A. E. Wickendon, *J. Appl. Phys.* **105**, 094316 (2009)
[18] M. S. Dresselhaus and P. C. Klund*, Advances in Physics* **49**, No. 6, 705-814 (2000)
[19] W. Ebbesen, H.J. Lezec, H.F. Ghaemi, T. Thio, and P.A. Wolff, *Nature* **391**, 667–669 (1998)
[20] Beerman, et. al. , *J. Opt. Soc. Am. B* **28**, 372-378 (2011)
[21] Genov, et. al., *Nano Letters* **4**, 153-158 (2004)
[22] J.B. Pendry, L. Martin-Moreno, F.J. Garcia-Vidal, *Science* **305**, 847 (2004)
[23] Moussavi et. al. *Phys. Rev. Lett*. **105**, 176803 (2010)
[24] Yu et. al., *Nature Materials* **9**, 730-735 (2010)
[25] M. Aizawa and J. M. Buriak, *Chem. Mater.* **19** (21), 5090 (2007)